nature medicine

Immune complexes stimulate CCR7-dependent dendritic cell migration to lymph nodes

Menna R Clatworthy[1,2], Caren E Petrie Aronin[2], Rebeccah J Mathews[1], Nicole Y Morgan[3], Kenneth G C Smith[4] & Ronald N Germain[2]

Antibodies are critical for defense against a variety of microbes, but they may also be pathogenic in some autoimmune diseases. Many effector functions of antibodies are mediated by Fcγ receptors (FcγRs), which are found on most immune cells, including dendritic cells (DCs)—important antigen-presenting cells that play a central role in inducing antigen-specific tolerance or immunity[1,2]. Following antigen acquisition in peripheral tissues, DCs migrate to draining lymph nodes via the lymphatics to present antigen to T cells. Here we demonstrate that FcγR engagement by IgG immune complexes (ICs) stimulates DC migration from peripheral tissues to the paracortex of draining lymph nodes. *In vitro*, IC-stimulated mouse and human DCs showed greater directional migration in a chemokine (C-C) ligand 19 (CCL19) gradient and increased chemokine (C-C) receptor 7 (CCR7) expression. Using intravital two-photon microscopy, we observed that local administration of IC resulted in dermal DC mobilization. We confirmed that dermal DC migration to lymph nodes depended on CCR7 and increased in the absence of the inhibitory receptor FcγRIIB. These observations have relevance to autoimmunity because autoantibody-containing serum from humans with systemic lupus erythematosus (SLE) and from a mouse model of SLE also increased dermal DC migration *in vivo*, suggesting that this process may occur in lupus, potentially driving the inappropriate localization of autoantigen-bearing DCs.

Antibodies have direct protective effects via pathogen or toxin neutralization and can activate complement or ligate Fc receptors[3,4]. FcγRs bind immune-complexed IgG and include activating receptors (in humans: FcγRIIA, FcγRIIIA and FcγRIIIB) and a single inhibitory receptor, FcγRIIB[5]. DCs express a number of receptors, among them FcγRs, which allow antigen internalization for processing and presentation to T cells[1,2,6]. Recognition of this displayed antigen may induce T cell tolerance or activation, a cellular decision influenced by the provision of co-stimulatory signals present on mature but not immature DCs[7,8]. Maturation of DCs may be driven by a variety of stimuli, including Toll-like receptor ligands and proinflammatory cytokines or activating FcγR cross-linking[9,10]. FcγRIIB provides a basal level of inhibition to DC maturation in the presence of ICs, thereby regulating immunogenic antigen presentation to T cells and providing an important tolerance checkpoint[11–15]. A number of stimuli preferentially reduce FcγRIIB expression on monocytes, notably interferon-γ (IFN-γ)[16], allowing these cells to be activated and matured by subsequent encounters with ICs. Deficiency or dysfunction of FcγRIIB confers susceptibility to the IC-mediated autoimmune disease SLE in both mice and humans[17–22].

To permit interactions with T cells, tissue-resident DCs not only need to be mature but also must relocate from peripheral tissues to lymph nodes[23–26]. Studies to date on the role of FcγRs in DCs have focused on the effects of antibody and FcγR cross-linking on DC maturation, but none has addressed the question of how antibody engagement of FcγRs might affect the migration and anatomical repositioning of DCs.

To determine if FcγR cross-linking with ICs might alter DC migration from peripheral tissue to lymph nodes, we stimulated bone marrow–derived DCs with ovalbumin (OVA) or IgG-opsonized OVA (ICs) for 24 h and subsequently transferred the DCs subcutaneously to a recipient mouse. We harvested draining lymph nodes 48 h following DC transfer and assessed DC migration by histological quantification. Exposure to OVA alone resulted in a limited number of wild-type DCs within the lymph node paracortex, whereas IC stimulation yielded a substantially greater number (**Fig. 1a**). We next used FcγRIIB-deficient DCs to model the effect of administering IC to activated DCs (on which FcγRIIB is downregulated[11–13]) or DCs from individuals with dysfunctional FcγRIIB[21]. Forty-eight hours after DC transfer, we observed higher numbers of IC-stimulated *Fcgr2b*$^{-/-}$ DCs than IC-stimulated wild-type DCs in the lymph node paracortex (**Fig. 1a–c**). To control for variations in DC administration and local tissue anatomy, we also co-transferred wild-type and FcγRIIB-deficient DCs into a single site. These experiments confirmed increased migration of IC-stimulated *Fcgr2b*$^{-/-}$ DCs to lymph nodes (**Fig. 1d,e**), as did lymph node disruption and DC enumeration by flow cytometry (**Fig. 1f**). We verified the viability of migrating DC by intravital imaging of lymph nodes (**Supplementary Video 1**) and by flow cytometry (**Supplementary Fig. 1**).

[1]Department of Medicine, MRC Laboratory of Molecular Biology, University of Cambridge, Cambridge, UK. [2]Laboratory of Systems Biology, Lymphocyte Biology Section, National Institute of Allergy and Infectious Diseases, National Institutes of Health, Bethesda, Maryland, USA. [3]Biomedical Engineering and Physical Sciences Resource, Microfabrication and Microfluidics Unit, National Institute of Biomedical Imaging and Bioengineering, National Institutes of Health, Bethesda, Maryland, USA. [4]Cambridge Institute for Medical Research and Department of Medicine, University of Cambridge School of Clinical Medicine, Cambridge, UK. Correspondence should be addressed to M.R.C. (mrc38@cam.ac.uk) or R.N.G. (rgermain@nih.gov).

Received 13 July; accepted 25 August; published online 10 November 2014; doi:10.1038/nm.3709

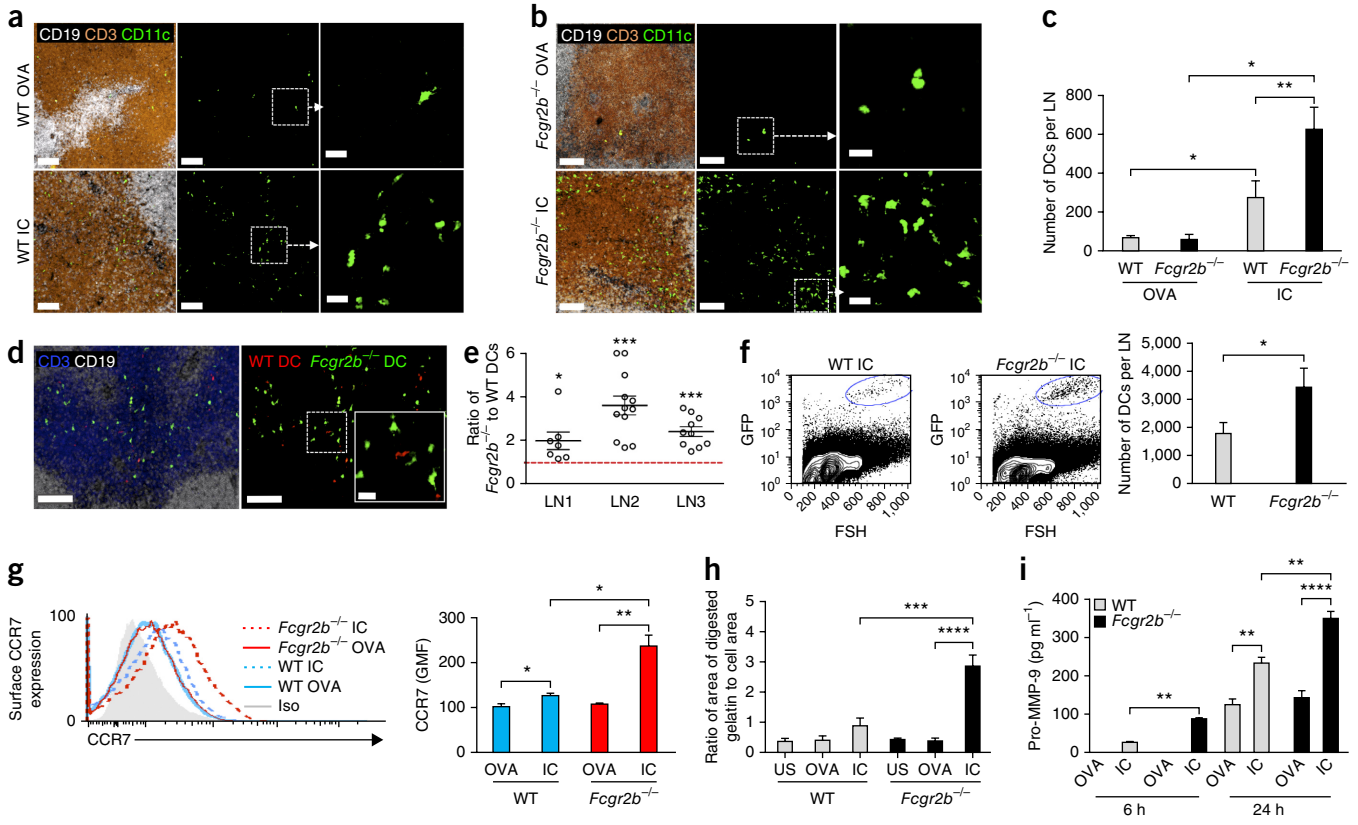

Figure 1 ICs increase CCR7 expression, matrix metalloprotease production and migration of mouse bone marrow–derived DCs. (**a**,**b**) Representative images of a draining lymph node 48 h after subcutaneous transfer of bone marrow–derived DCs (BMDCs) (green) from wild type (WT) (**a**) or *Fcgr2b*$^{-/-}$ (**b**) mice incubated with OVA (top panels) or IgG-opsonized ovalbumin (IC, bottom panels) for 24 h before transfer. B cell follicles (CD19) shown in white and T cells (CD3) in brown. Scale bars in left and middle panels are 80 μm. Right panels show high-power image (scale bars, 20 μm). (**c**) Total number of WT and *Fcgr2b*$^{-/-}$ DCs per lymph node 48 h after transfer, as enumerated from serial 50-μm sections. Graph shows mean and s.e.m. of values obtained from six lymph nodes per experimental condition. LN, lymph node. (**d**) Representative images of draining lymph node 48 h after transfer of BMDCs from WT (red) and *Fcgr2b*$^{-/-}$ (green) mice stimulated for 24 h with IC. B cells are stained with CD19 (white) and T cells with CD3 (blue). Scale bars, 100 μm. Inset shows high-power image of area outlined by white dashed square (scale bar, 20 μm). (**e**) Ratio of *Fcgr2b*$^{-/-}$ to IC-stimulated WT BMDCs in the paracortex of three LNs 48 h after subcutaneous transfer. Each point represents the ratio observed in a 50-μm section. Bars show mean and s.e.m. Red dashed line marks a ratio of 1 (value of equivalent DC migration). (**f**) Representative flow cytometric data from dissociated lymph nodes 48 h after transfer of GFP^{+} mouse BMDCs. Left, IC-stimulated WT BMDCs; middle, *Fcgr2b*$^{-/-}$ BMDCs; right, quantification of LN BMDCs by flow cytometry 48 h after transfer (mean and s.e.m. from seven lymph nodes from four mice in each experimental condition). FSH, forward scatter height. (**g**) Representative histograms of CCR7 expression on WT (blue lines) and *Fcgr2b*$^{-/-}$ (red lines) BMDCs after 24-h incubation with OVA (solid lines) or IC (dotted lines) (left). Isotype control antibody shown in gray filled histogram. Geometric mean fluorescence (GMF) of CCR7 staining in WT and *Fcgr2b*$^{-/-}$ BMDCs (right). Values show mean and s.e.m. of triplicates of each experimental condition and are representative of three experimental replicates. (**h**) Gelatinase production as quantified by area of FITC gelatin digested over 24 h by DCs following FcγR cross-linking with IC. Graph shows mean and s.e.m. values obtained from combined result of three separate experiments for each condition. US, unstimulated. (**i**) MMP-9 levels in culture supernatants obtained from WT and *Fcgr2b*$^{-/-}$ BMDCs 6 and 24 h after incubation with OVA or IC. Graph shows mean and s.e.m. of triplicates for each experimental condition from a representative experiment of three repeats. *P* values throughout calculated using a Student's *t*-test (two-tailed). $^{*}P \le 0.05$, $^{**}P \le 0.01$, $^{***}P \le 0.001$, $^{****}P \le 0.0001$.

To dissect the mechanisms underpinning IC-induced DC migration, we considered a variety of factors known to affect this process. In particular, DCs express CCR7, which interacts with CCL19 and CCL21 expressed on lymphatics[25,26]. IC stimulation resulted in a modest upregulation of CCR7 expression on wild-type DCs but a substantial upregulation on FcγRIIB-deficient DCs (**Fig. 1g**). A second factor we considered was the production of matrix metalloproteinases (MMPs) because migrating DCs secrete MMPs, particularly MMP-2 and MMP-9 (refs. 27,28), to facilitate movement through the extracellular matrix and across basement membranes. Pharmacological inhibition[29], antibody neutralization[30] or genetic deletion of MMPs[27,28,31] reduces DC migration. *In vitro*, within 4 h of FcγR cross-linking, wild-type DCs produced proteases capable of gelatin digestion (**Fig. 1h** and **Supplementary Fig. 2**). This response was greater in FcγRIIB-deficient DCs (**Fig. 1h**), as were levels of MMP-9 in DC culture supernatants (**Fig. 1i**). IC-induced MMP-9 production by mouse DCs was abrogated by inhibition of the kinase ERK but not JNK or p38 (**Supplementary Fig. 3**).

To further explore the possible role of IC-induced upregulation of CCR7 on DC chemotaxis, we used a three-dimensional *in vitro* model, embedding IC-stimulated DCs within a collagen matrix (**Fig. 2a**) in a rising soluble CCL19 gradient (C.E.P.A., J.S. Yoon, N.Y.M., T. Prustel, M. Meier-Schellersheim & R.N.G. unpublished results). IC-stimulated wild-type DCs showed greater migration toward CCL19 than OVA-stimulated DCs (**Fig. 2b–d**, **Supplementary Fig. 4**,

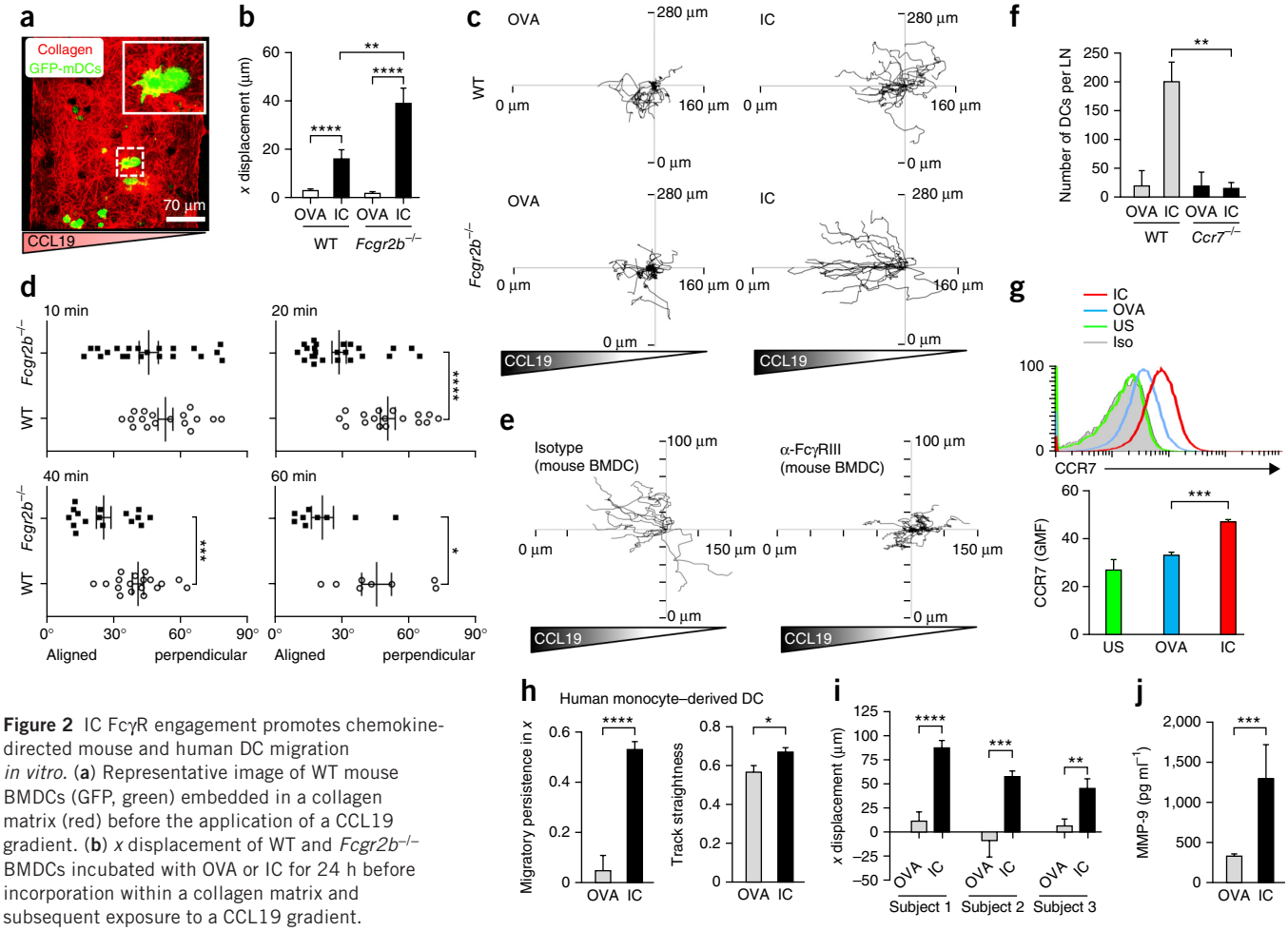

Figure 2 IC FcγR engagement promotes chemokine-directed mouse and human DC migration *in vitro*. (**a**) Representative image of WT mouse BMDCs (GFP, green) embedded in a collagen matrix (red) before the application of a CCL19 gradient. (**b**) *x* displacement of WT and *Fcgr2b*$^{-/-}$ BMDCs incubated with OVA or IC for 24 h before incorporation within a collagen matrix and subsequent exposure to a CCL19 gradient. Graphs show mean and s.e.m. of values obtained from one collagen gel, representative of three experimental replicates per condition with 15–20 cells tracked per gel. (**c**) Representative migration tracks in a CCL19 gradient of WT (top panels) and *Fcgr2b*$^{-/-}$ (bottom panels) BMDCs incubated with OVA (left panels) or IC (right panels) for 24 h before suspension in the collagen matrix. (**d**) Angle of leading protrusion relative to chemokine gradient of WT (open circles) and *Fcgr2b*$^{-/-}$ (filled squares) BMDCs suspended in a collagen matrix at 10, 20, 40 and 60 min after application of CCL19 gradient. Angles closer to 0° indicate cell polarization parallel to the gradient. Each symbol represents a cell in a single collagen gel, representative of three experimental replicates per condition. Horizontal lines show mean; error bars are s.e.m. (**e**) Representative migration tracks in a CCL19 gradient of BMDCs incubated with IC, either in the presence of an FcγRIII-blocking antibody (right) or an isotype control antibody (left). (**f**) Quantification of the number of WT and *Ccr7*$^{-/-}$ DCs within draining lymph nodes 48 h after subcutaneous transfer. Mean and s.e.m. from six lymph nodes from three mice in each experimental group shown. (**g**) CCR7 expression on human monocyte–derived DCs incubated with OVA (blue line) or IC (red line) for 24 h, or unstimulated DC incubated in medium alone (US). Isotype control antibody staining (Iso) shown in gray filled histogram. Representative histograms of CCR7 surface expression, as measured by relative fluorescence intensity, are shown at the top, and geometric mean fluorescence (GMF) and s.e.m. of GMF of triplicate samples for each experimental condition, from one of three replicates are shown at the bottom. (**h**) Migratory persistence along the *x* dimension (left) and track straightness (right) of human monocyte–derived DCs in a human CCL19 gradient following incubation with OVA or IC for 24 h prior. Values represent the mean and s.e.m. from 15–20 cells migrating in at least three collagen gels per subject and from three healthy subjects. (**i**) *x* displacement of human monocyte–derived DCs from three subjects following application of a CCL19 gradient. Mean and s.e.m. of 15–20 cells per stimulation, representative of three experimental repeats. (**j**) Concentration of MMP-9 in culture supernatants obtained from human monocyte–derived DCs isolated from three healthy subjects. Values represent the mean and s.e.m. of triplicates for each condition. In **c** and **e**, tracks are derived from 15–20 cells in a single collagen gel for each condition and are representative of three similar experiments. *P* values throughout calculated using a Student's *t*-test (two-tailed). *$P \leq 0.05$, **$P \leq 0.01$, ***$P \leq 0.001$, ****$P \leq 0.0001$.

Supplementary Videos 2 and **3**). In the absence of FcγRIIB, IC-stimulated DCs showed even greater directional migration (**Fig. 2b–d**, **Supplementary Fig. 4**, **Supplementary Videos 4** and **5**). The capacity of IC to stimulate mouse DC chemotaxis was dependent on the activating FcγR, FcγRIII (**Fig. 2e**, **Supplementary Fig. 5a**), as was IC-mediated upregulation of CCR7 and MMP-9 (**Supplementary Fig. 5b**,**c**). CCR7 deficiency abrogated IC-induced DC migration to draining lymph nodes following subcutaneous transfer (**Fig. 2f** and **Supplementary Fig. 6**).

To determine the relevance to humans, we generated DCs from peripheral blood monocytes obtained from healthy donors. These DCs demonstrated a significant increase in CCR7 expression post-stimulation with ICs (**Fig. 2g**), increased directional migration in a CCL19 gradient (**Fig. 2h**,**i**, **Supplementary Videos 6** and **7**) and increased production of MMP-9 (**Fig. 2j**).

Given our quantitative migration data in the DC transfer model and the *in vitro* data, we wished to determine whether the administration of ICs was sufficient to stimulate endogenous DC

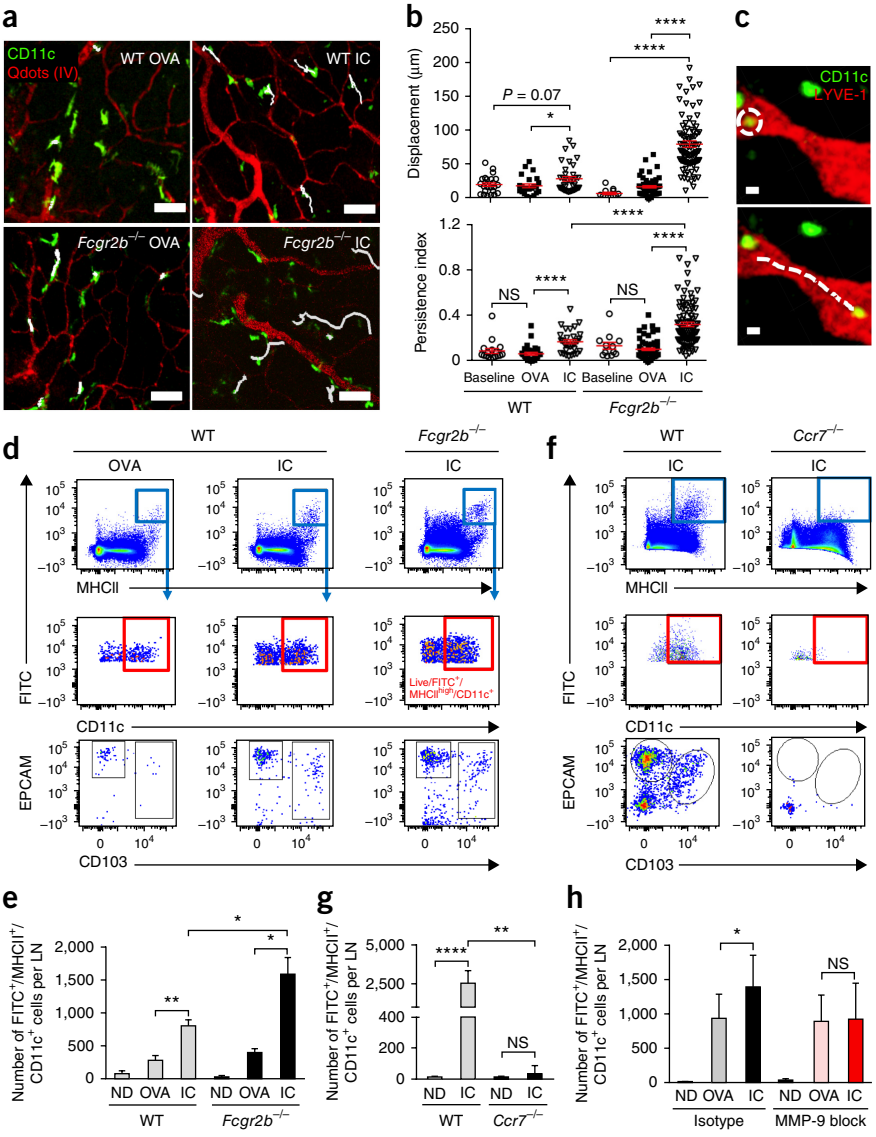

Figure 3 ICs stimulate CCR7-dependent dermal DC migration to lymph nodes *in vivo*. (**a**) Footpad dermal DCs (green) were imaged by two-photon microscopy in WT CD11cEYFP (top panels) and *Fcgr2b*$^{-/-}$ CD11cEYFP mice (bottom panels) 16 h after administration of OVA or IC subcutaneously to the footpad. Blood vessels are shown in red (Qdots intravenous), and cell tracks over an 80-min period are shown in white. Scale bars, 50 μm. (**b**) Quantification of displacement and persistence index for dermal DCs 16 h after OVA or IC administration. Each symbol represents single DC. Images obtained from the footpads of three mice per experimental group. NS, nonsignificant. (**c**) Sequential images obtained by intravital two-photon microscopy of the footpad 16 h after IC administration. Movement of a dermal DC (green) tracked (white dashed line) through a dermal lymphatic vessel (LYVE-1, red). Scale bars, 10 μm. Horizontal lines show mean; error bars show s.e.m. (**d**–**g**) Representative flow cytometric plots and quantification of live FITC^{+} MHCII^{high} CD11c^{+} cells in draining lymph nodes in WT and *Fcgr2b*$^{-/-}$ mice (**d**,**e**) and WT and *Ccr7*$^{-/-}$ mice (**f**,**g**) 48 h after application of FITC to skin followed by intradermal administration of OVA or IC as indicated. Mean and s.e.m. DC number observed in lymph nodes obtained from four mice per experimental condition. *P* values calculated using a Student's *t*-test (two-tailed).EPCAM, epithelial cell adhesion molecule; ND, non-draining lymph node. (**h**) Quantification of live FITC^{+} MHCII^{high} CD11c^{+} cells present in draining lymph nodes of WT mice treated with MMP-9-blocking antibody or isotype control before application of FITC to skin with intradermal administration of OVA or IC. Mean and s.e.m. DC number observed in lymph nodes obtained from four mice per experimental condition. *P* values throughout calculated using a paired *t*-test to compare lymph nodes draining skin treated with OVA (left inguinal) and IC (right inguinal) or nondraining lymph nodes (brachial) from the same mouse. $^{*}P \leq 0.05$, $^{**}P \leq 0.01$, $^{***}P \leq 0.001$, $^{****}P \leq 0.0001$.

migration *in vivo*. Utilizing intravital two-photon microscopy to assess the dynamic behavior of dermal DCs in CD11cEYFP mice, we found that administration of IC into the footpad resulted in mobilization of these cells (consistent with chemotaxis or chemokinesis), whereas injection of OVA alone did not (**Fig. 3a**,**b** and **Supplementary Videos 8** and **9**). These cells did not express granulocyte or monocyte markers (**Supplementary Fig. 7**), and we observed them clustering around, entering into and traveling within lymphatic vessels following IC stimulation (**Fig. 3c**, **Supplementary Video 10**, **Supplementary Figs. 8** and **9**). IC-induced dermal DC mobilization was even greater in *Fcgr2b*$^{-/-}$ CD11cEYFP mice (**Fig. 3a**,**b**, **Supplementary Videos 11** and **12**), supporting the idea that human subjects with FcγRIIB dysfunction might demonstrate increased IC-induced DC motility.

Intravital imaging of skin DCs only allows the visualization of the initial phase of DC migration; therefore, we sought to determine whether IC-stimulated dermal DCs complete their journey to draining lymph nodes. We used FITC painting to label dermal DCs, and followed this with local administration of OVA or IC. In wild-type mice, a substantially greater number of FITC^{+} MHC class II^{high} CD11c^{+} cells were present in draining lymph nodes after IC stimulation than after OVA stimulation (**Fig. 3d**,**e**), and these cells expressed markers typical of skin-resident, migratory DCs (**Fig. 3d**). We observed greater accumulation of FITC-labeled DCs in *Fcgr2b*$^{-/-}$ mice following IC stimulation (**Fig. 3d**,**e**). CCR7-deficient dermal DCs showed severely impaired migration to draining lymph nodes in response to IC stimulation (**Fig. 3f**,**g** and **Supplementary Fig. 10**). MMP-9 blockade had a less potent effect than CCR7 deficiency on IC-mediated dermal DC migration (**Fig. 3h**, **Supplementary Fig. 11**).

Because local administration of IC induced DC migration *in vivo*, we hypothesized that this phenomenon would have relevance to SLE, a disease characterized by IC deposition in tissues, including skin[32]. Of note, abnormalities in monocytes and DCs have been observed in patients with lupus[33–36]. To address whether ICs derived from individuals with lupus might stimulate DC mobilization *in vivo*, we injected heat-inactivated serum, taken either from NZB/W F_1 mice with antinuclear antibodies and nephritis, a mouse model of human SLE, or from undiseased aged-matched controls, into the footpads of CD11cEYFP mice. Serum from NZB/W F_1 mice with lupus stimulated dermal DC mobilization (**Fig. 4a**,**b** and **Supplementary Video 13**), whereas control serum did not (**Fig. 4a**,**b**, **Supplementary Video 14**

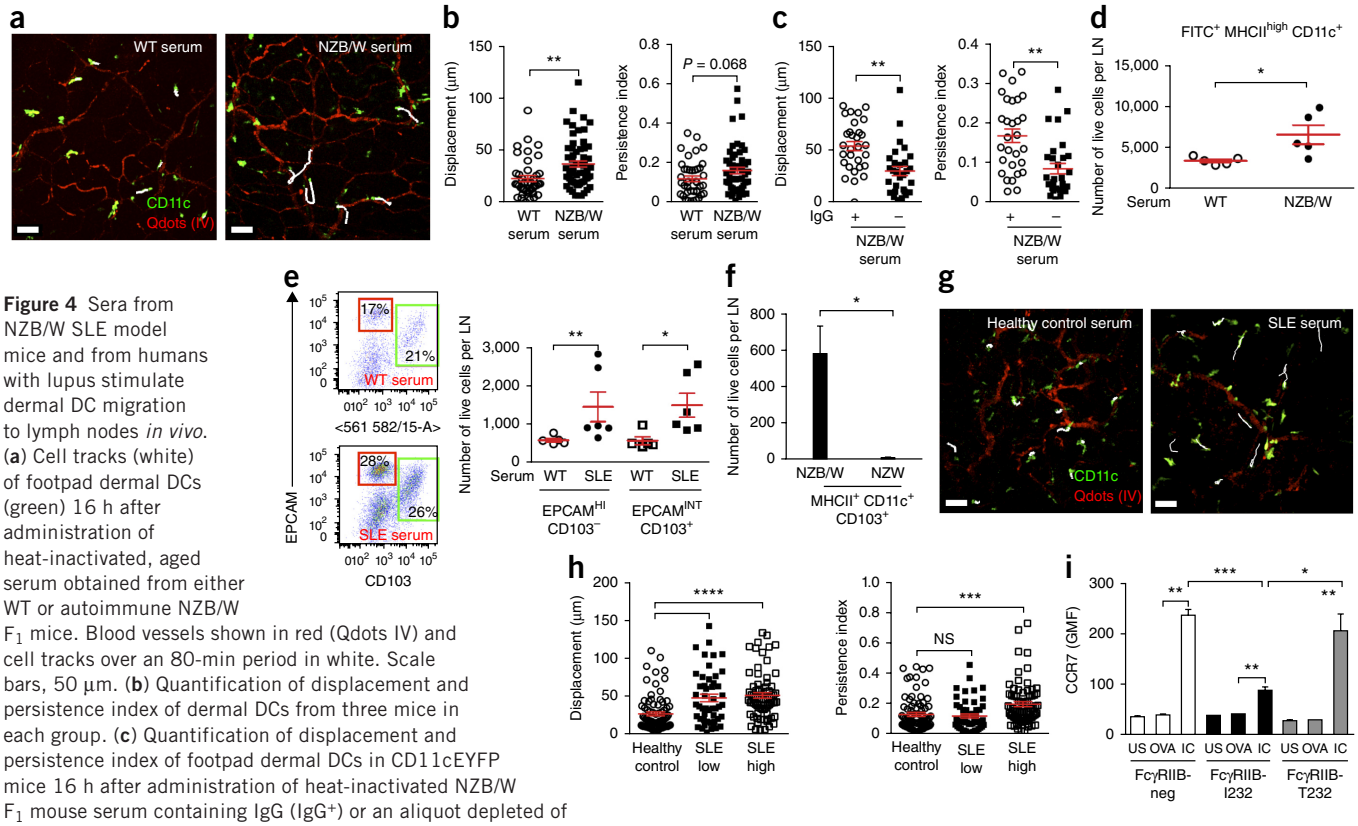

Figure 4 Sera from NZB/W SLE model mice and from humans with lupus stimulate dermal DC migration to lymph nodes *in vivo*. (**a**) Cell tracks (white) of footpad dermal DCs (green) 16 h after administration of heat-inactivated, aged serum obtained from either WT or autoimmune NZB/W F_1 mice. Blood vessels shown in red (Qdots IV) and cell tracks over an 80-min period in white. Scale bars, 50 μm. (**b**) Quantification of displacement and persistence index of dermal DCs from three mice in each group. (**c**) Quantification of displacement and persistence index of footpad dermal DCs in CD11cEYFP mice 16 h after administration of heat-inactivated NZB/W F_1 mouse serum containing IgG (IgG$^+$) or an aliquot depleted of IgG (IgG$^-$). (**d**) Number of live FITC$^+$ MHCII^{high} CD11c$^+$ cells per draining lymph node in WT mice. (**e**) Representative flow cytometric plots (left) and quantification (right) of FITC$^+$ MHCII^{high} CD11c$^+$ EPCAM$^+$ (Langerhans cells, circles) and CD11c$^+$ CD103$^+$ (dermal DCs, squares) in draining lymph nodes 48 h after application of FITC to skin in mice given heat-inactivated WT (open symbols) or serum from NZB/W mice with SLE (black symbols) serum intraperitoneally 12 h previously. Each circle in **d** and **e** represents quantification from a single lymph node. (**f**) Number of MHCII^{high} CD11c$^+$ CD103$^+$ cells in renal lymph nodes of aged NZB/W mice with lupus nephritis and aged-match NZW controls. Graphs show mean and s.e.m. of lymph nodes taken from four mice. (**g**) Representative cell tracks (white) of footpad dermal DCs (green). Scale bars, 50 μm. (**h**) Quantification of displacement and persistence index of dermal DCs in WT mice 16 h after administration of heat-inactivated serum obtained from healthy controls or patients with SLE. Graphs show values from mice treated with three healthy control sera (open circles), from three patients with SLE who had low disease activity (British Isles Lupus Assessment Group (BILAG) scores 2–9, filled squares, 'SLE low') or from three patients with SLE who had high disease activity (BILAG scores 15–21, open squares, 'SLE high'). (**i**) CCR7 expression on WT U937 cells or those stably expressing FcγRIIB-I232 or FcγRIIB-T232 24 h after incubation with OVA or IC. Graph shows mean and s.e.m. of duplicates for each experimental condition, representative of three experimental replicates. In **b**, **c** and **h** each point represents a single dermal DC, imaged 16 h after administration of serum. Images obtained from the footpads of three mice per experimental condition. Bar shows the mean value. Horizontal lines show mean; error bars show s.e.m. *P* values throughout calculated using a Student's *t*-test (two-tailed). $^*P \le 0.05$, $^{**}P \le 0.01$, $^{***}P \le 0.001$, $^{****}P \le 0.0001$. NS, nonsignificant.

and **Supplementary Fig. 12a**,**b**). The stimulatory effect of the serum from NZB/W F_1 mice with lupus on dermal DC motility was IgG dependent (**Fig. 4c** and **Supplementary Fig. 12c**). We also observed a greater number of FITC-labeled dermal DCs in the draining lymph nodes of mice to which serum from NZB/W F_1 mice with lupus had been transferred intraperitoneally than in those of mice given wild-type serum (**Fig. 4d**,**e**). In addition, in renal draining lymph nodes of aged NZB/W F_1 mice with lupus nephritis, the number of migratory DCs (CD11c$^+$ MHCII^{high} CD103$^+$) was substantially greater than that in aged-match NZW control mice, in which such cells were scarcely detectable (**Fig. 4f** and **Supplementary Fig. 13**).

To explore the relevance of these observations to human disease, we administered heat-inactivated serum from human patients with lupus into the footpads of CD11cEYFP mice. This resulted in greater dermal DC migration (increased displacement and a higher persistence index) than injection of healthy control serum, particularly when the serum was obtained from patients with high disease activity scores (**Fig. 4g**,**h**, **Supplementary Fig. 14**, **Supplementary Videos 15** and **16**). In addition, we examined the effect of a polymorphism in human *FCGR2B* (rs1050501) on DC CCR7 expression. This polymorphism involves an amino acid substitution in the transmembrane domain, a threonine replacing an isoleucine (FcγRIIB-T232), resulting in receptor dysfunction[21,22] and contributing to lupus susceptibility[37]. U937 human monocytic cells stably transfected with FcγRIIB-I232 or FcγRIIBT232 (ref. 21) were differentiated to a DC phenotype and stimulated with IC. Cells transfected with the dysfunctional FcγRIIBT232 had higher IC-dependent CCR7 expression than cells transfected with FcγRIIBI232 (**Fig. 4i**), suggesting that DCs from individuals with the lupus-associated polymorphism would show increased migration when exposed to ICs, analogous to our observations in *Fcgr2b*$^{-/-}$ mice.

In conclusion, our study demonstrates a previously unknown effect of antibody opsonization, namely increased DC migration to lymph nodes via FcγR-induced upregulation of CCR7 and MMPs. This would allow the optimal positioning of DCs in the lymph node paracortex, acting synergistically with the known effects of FcγR cross-linking on MHC class II and co-stimulatory molecule upregulation on these cells, to promote immunogenic T cell–DC interactions. Furthermore, we

show that dermal DC migration is increased following administration of ICs or autoantibody-containing serum, and this effect is particularly pronounced in the absence of the inhibitory receptor FcγRIIB, a known susceptibility locus in SLE. Together, these data suggest an additional mechanism by which ICs might drive autoimmunity in SLE via the inappropriate localization of autoantigen-bearing DCs and may also have implications for boost strategies in vaccination, since measures to block or downregulate FcγRIIB at the time of boost would enhance the migration of immunogen-bearing DCs to lymph nodes, thereby increasing T cell activation and the magnitude of the vaccine response.

METHODS

Methods and any associated references are available in the online version of the paper.

Note: Any Supplementary Information and Source Data files are available in the online version of the paper.

ACKNOWLEDGMENTS

This work was supported by a Wellcome Trust Intermediate Fellowship (WT081020) to M.R.C. and by the National Institute for Health Research Cambridge Biomedical Research Centre and the Intramural Research Program of the US National Institute of Allergy and Infectious Diseases, part of the US National Institutes of Health. We thank J. Yoon for technical advice and M. Espeli for helpful discussions.

AUTHOR CONTRIBUTIONS

M.R.C. conceived of the project, carried out experiments, designed and supervised experiments, analyzed data and wrote the manuscript. C.E.P.A. and R.J.M. carried out experiments and analyzed data. N.Y.M. provided technical advice to C.E.P.A. for the *in vitro* DC chemotaxis assay. K.G.C.S. provided mentorship for M.R.C. and scientific advice. R.N.G. provided advice on experimental design, assisted with manuscript writing and editing and provided mentorship for M.R.C. and C.E.P.A.

COMPETING FINANCIAL INTERESTS

The authors declare no competing financial interests.

1. Banchereau, J. & Steinman, R.M. Dendritic cells and the control of immunity. *Nature* **392**, 245–252 (1998).
2. Steinman, R.M. Decisions about dendritic cells: past, present, and future. *Annu. Rev. Immunol.* **30**, 1–22 (2012).
3. Krause, R.M., Dimmock, N.J. & Morens, D.M. Summary of antibody workshop: the role of humoral immunity in the treatment and prevention of emerging and extant infectious diseases. *J. Infect. Dis.* **176**, 549–559 (1997).
4. Joller, N., Weber, S.S. & Oxenius, A. Antibody-Fc receptor interactions in protection against intracellular pathogens. *Eur. J. Immunol.* **41**, 889–897 (2011).
5. Ravetch, J.V. & Bolland, S. IgG Fc receptors. *Annu. Rev. Immunol.* **19**, 275–290 (2001).
6. Itano, A.A. *et al.* Distinct dendritic cell populations sequentially present antigen to CD4 T cells and stimulate different aspects of cell-mediated immunity. *Immunity* **19**, 47–57 (2003).
7. Hawiger, D. *et al.* Dendritic cells induce peripheral T cell unresponsiveness under steady state conditions *in vivo*. *J. Exp. Med.* **194**, 769–779 (2001).
8. Steinman, R.M., Hawiger, D. & Nussenzweig, M.C. Tolerogenic dendritic cells. *Annu. Rev. Immunol.* **21**, 685–711 (2003).
9. Roake, J.A. *et al.* Dendritic cell loss from nonlymphoid tissues after systemic administration of lipopolysaccharide, tumor necrosis factor, and interleukin 1. *J. Exp. Med.* **181**, 2237–2247 (1995).
10. Reis e Sousa, C. Dendritic cells in a mature age. *Nat. Rev. Immunol.* **6**, 476–483 (2006).
11. Boruchov, A.M. *et al.* Activating and inhibitory IgG Fc receptors on human dendritic cells mediate opposing functions. *J. Clin. Invest.* **115**, 2914–2923 (2005).
12. Dhodapkar, K.M. *et al.* Selective blockade of inhibitory Fcγ receptor enables human dendritic cell maturation with IL-12p70 production and immunity to antibody-coated tumor cells. *Proc. Natl. Acad. Sci. USA* **102**, 2910–2915 (2005).
13. Dhodapkar, K.M. *et al.* Selective blockade of the inhibitory Fcγ receptor (FcγRIIB) in human dendritic cells and monocytes induces a type I interferon response program. *J. Exp. Med.* **204**, 1359–1369 (2007).
14. Kalergis, A.M. & Ravetch, J.V. Inducing tumor immunity through the selective engagement of activating Fcγ receptors on dendritic cells. *J. Exp. Med.* **195**, 1653–1659 (2002).
15. van Montfoort, N. *et al.* Fcγ receptor IIb strongly regulates fcγ receptor-facilitated T cell activation by dendritic cells. *J. Immunol.* **189**, 92–101 (2012).
16. Pricop, L. *et al.* Differential modulation of stimulatory and inhibitory Fcγ receptors on human monocytes by Th1 and Th2 cytokines. *J. Immunol.* **166**, 531–537 (2001).
17. Smith, K.G.C. & Clatworthy, M.R. FcγRIIB in autoimmunity and infection: evolutionary and therapeutic implications. *Nat. Rev. Immunol.* **10**, 328–343 (2010).
18. Bolland, S. & Ravetch, J.V. Spontaneous autoimmune disease in FcγRIIB-deficient mice results from strain-specific epistasis. *Immunity* **13**, 277–285 (2000).
19. Brownlie, R.J. *et al.* Distinct cell-specific control of autoimmunity and infection by FcγRIIB. *J. Exp. Med.* **205**, 883–895 (2008).
20. Boross, P. *et al.* The inhibiting Fc receptor for IgG, FcγRIIB, is a modifier of autoimmune susceptibility. *J. Immunol.* **187**, 1304–1313 (2011).
21. Floto, R.A. *et al.* Loss of function of a lupus-associated FcγRIIB polymorphism through exclusion from lipid rafts. *Nat. Med.* **11**, 1056–1058 (2005).
22. Kono, H. *et al.* FcγRIIB Ile232Thr transmembrane polymorphism associated with human systemic lupus erythematosus decreases affinity to lipid rafts and attenuates inhibitory effects on B cell receptor signaling. *Hum. Mol. Genet.* **14**, 2881–2892 (2005).
23. Randolph, G.J., Angeli, V. & Swartz, M.A. Dendritic-cell trafficking to lymph nodes through lymphatic vessels. *Nat. Rev. Immunol.* **5**, 617–628 (2005).
24. Cyster, J.G. Chemokines and the homing of dendritic cells to the T cell areas of lymphoid organs. *J. Exp. Med.* **189**, 447–450 (1999).
25. Förster, R. *et al.* CCR7 coordinates the primary immune response by establishing functional microenvironments in secondary lymphoid organs. *Cell* **99**, 23–33 (1999).
26. Sallusto, F. *et al.* Rapid and coordinated switch in chemokine receptor expression during dendritic cell maturation. *Eur. J. Immunol.* **28**, 2760–2769 (1998).
27. Ratzinger, G. *et al.* Matrix metalloproteinases 9 and 2 are necessary for the migration of Langerhans cells and dermal dendritic cells from human and murine skin. *J. Immunol.* **168**, 4361–4371 (2002).
28. Yen, J.H., Khayrullina, T. & Ganea, D. PGE2-induced metalloproteinase-9 is essential for dendritic cell migration. *Blood* **111**, 260–270 (2008).
29. Lebre, M.C., Kalinski, P., Das, P.K. & Everts, V. Inhibition of contact sensitizer-induced migration of human Langerhans cells by matrix metalloproteinase inhibitors. *Arch. Dermatol. Res.* **291**, 447–452 (1999).
30. Kobayashi, Y., Matsumoto, M., Kotani, M. & Makino, T. Possible involvement of matrix metalloproteinase-9 in Langerhans cell migration and maturation. *J. Immunol.* **163**, 5989–5993 (1999).
31. Ichiyasu, H. *et al.* Matrix metalloproteinase-9-deficient dendritic cells have impaired migration through tracheal epithelial tight junctions. *Am. J. Respir. Cell Mol. Biol.* **30**, 761–770 (2004).
32. Rahman, A. & Isenberg, D.A. Systemic lupus erythematosus. *N. Engl. J. Med.* **358**, 929–939 (2008).
33. Blanco, P., Palucka, A.K., Gill, M., Pascual, V. & Banchereau, J. Induction of dendritic cell differentiation by IFN-α in systemic lupus erythematosus. *Science* **294**, 1540–1543 (2001).
34. Decker, P., Kotter, I., Klein, R., Berner, B. & Rammensee, H.G. Monocyte-derived dendritic cells over-express CD86 in patients with systemic lupus erythematosus. *Rheumatology (Oxford)* **45**, 1087–1095 (2006).
35. Ding, D., Mehta, H., McCune, W.J. & Kaplan, M.J. Aberrant phenotype and function of myeloid dendritic cells in systemic lupus erythematosus. *J. Immunol.* **177**, 5878–5889 (2006).
36. Crispín, J.C., Vargas-Rojas, M.I., Monsivais-Urenda, A. & Alcocer-Varela, J. Phenotype and function of dendritic cells of patients with systemic lupus erythematosus. *Clin. Immunol.* **143**, 45–50 (2012).
37. Willcocks, L.C. *et al.* A defunctioning polymorphism in FCGR2B is associated with protection against malaria but susceptibility to systemic lupus erythematosus. *Proc. Natl. Acad. Sci. USA* **107**, 7881–7885 (2010).

ONLINE METHODS

Mice. FcγRIIB-deficient mice on a C57BL/6 background[18] were kindly provided by J. Ravetch (Rockefeller University) and S. Bolland (US National Institutes of Health, US National Institute of Allergy and Infectious Diseases (NIAID)) and crossed to transgenic mice expressing EGFP under the control of the human ubiquitin C promoter[38] (Jackson Laboratories) or transgenic mice expressing Venus EYFP under the control of the CD11c promoter[39] (obtained from M. Nussenzweig, Rockefeller University). C57BL/6 mice were obtained from Jackson Laboratories or from Charles River Laboratories (Margate, UK). NZB/W F_1 were bred in-house from NZB and NZW mice obtained from Harlan UK. CCR7-deficient mice on a C57BL/6 background (strain B6.129P2(C)-Ccr7^{tm1Rfor}/J, stock number 006621, live repository, aged 8 weeks) were purchased from Jackson Laboratories. Age-matched C57BL/6 JAX mice were used as controls. In all experiments, both male and female mice were used. Mice were maintained in specific pathogen–free conditions at an Association for Assessment and Accreditation of Laboratory Animal Care–accredited animal facility at NIAID or at a Home Office–approved facility in the UK. All procedures were approved by the NIAID Animal Care and Use Committee (US National Institutes of Health, Bethesda, MD) or were conducted in accordance with the United Kingdom Animals (Scientific Procedures) Act of 1986.

Antibodies. For immunofluorescence and flow cytometric studies, the following antibodies were used: mouse antibodies (from eBioscience unless otherwise indicated): anti-B220 antibody (clone RA3-6B2, product code 561877), anti-CD3 antibody (clone 17A2, 561389) (BD Biosciences, San Jose, California), PE-conjugated anti-mouse CCR7 (clone 4B12, 12-1971), PeCy7-conjugated anti-CD4 (clone RM4-5, 25-0042), PeCy7-conjugated anti-CD19 (clone eBio 1D3, 25-0193), FITC-conjugated anti-CD11b (clone M1/70, 53-0112) Alexa Fluor 780-conjugated CD11c (clone N418, 47-0114), Pacific Blue–conjugated anti-class II (clone AF6-120.1, 48-5320), PE-conjugated anti-CD103 (clone 2E7, 12-1031), APC-conjugated anti-EpCAM (clone G8.8, 17-5791), ef450-conjugated Gr-1 (clone RB6-8C5, 48-5931) and PE-conjugated Ly6C (Clone HK1.4, 12-5932).

Human antibodies (from BD Pharmingen unless otherwise indicated): PE-Cy7-conjugated anti-CCR7 (clone 3D12, 560922), PE-Cy7– conjugated Rat IgG2a isotype control (clone R35-95, 557855), APC-conjugated CD86 (clone 2331, 560956), FITC- conjugated HLA DR (clone G46-6, 560944).

All antibodies were used at 1/200 dilution (except for the MHC class II antibody, which was used at 1/100). For some flow cytometric studies, a Live/Dead Fixable Aqua Dead Cell Stain Kit (Invitrogen-Molecular Probes) was used.

Immune complexes. Endotoxin-free ovalbumin (EndoGrade Ovalbumin, Hyglos GmbH) was opsonized with a polyclonal rabbit anti-ovalbumin antibody (Sigma-Aldrich) at 37 °C for 1 h.

DC culture and stimulation. We generated primary mouse BMDCs as described previously[40]. Briefly, bone marrow was flushed from femurs and tibias, plated in regular petri dishes at 2.5×10^6 cells per dish and supplemented with 20 ng mL^{-1} granulocyte-macrophage colony–stimulating factor (GM-CSF, Peprotech) in base media (10% Hyclone FBS, 1% penicillin/streptomycin in RPMI 1640) 3 times over 8 d. On day 9, DCs were transferred to tissue culture plates and incubated overnight with endotoxin-free ovalbumin (EndoGrade Ovalbumin, Hyglos) or immune-complexed ovalbumin for 24 h at 37 °C.

We generated human monocyte–derived DCs from the peripheral blood of healthy volunteers. Samples were obtained with informed consent and the approval of the Cambridge Local Research Ethical committee (reference 08/H0308/176) or from normal volunteers from the US National Institutes of Health Blood Bank. Blood was subjected to Ficoll-Hypaque density separation to isolate peripheral blood mononuclear cells, and monocytes were enriched by negative selection by using a MACS-based monocyte purification kit (Miltenyi Biotec). DCs were generated by culturing the monocytes for 6 d with human GM-CSF (100 ng mL^{-1}, PeproTech) in DMEM supplemented with 10% heat-inactivated calf serum.

For mouse FcγR blocking studies, anti-mouse FcγRIII (CD16, AF1960) or goat anti-mouse isotype control (AB-108-C; both obtained from R&D Systems) were added to cells 1 h before stimulation with IC (final concentration 1.5 μg mL^{-1}). Similarly, the PI3K inhibitor (ZSTK474, Selleckchem, 100 nM) or Akt inhibitor (AKT-XI (3-Formylchromone thiosemicarbazone, Cu(II)Cl_2 Complex, FPA-124), Merck Millipore, 2.5 μM) was added to DCs before addition of IC, and cells and supernatants were harvested at 24 h.

Cell lines. The human monocytic cell line U937 (gift from R.A. Floto) cells stably transfected with vectors containing various isoforms of FcγRIIB (as described previously[21]) were used. Cells were cultured in RPMI 1640 with 10% FCS (Sigma) and penicillin/streptomycin (Sigma).

***In vivo* DC migration.** 24 h following culture with ovalbumin or immune-complexed ovalbumin, 5×10^6 BMDCs were washed in PBS to remove non-internalized ovalbumin or immune complexes and injected subcutaneously in the flank or footpad (depending on the lymph node harvested). 48 h following transfer, lymph nodes were harvested and processed for histological examination or flow cytometric analysis. Cells were labeled with Cell Tracker Orange (Invitrogen Molecular Probes) or Cell tracker Green (Invitrogen Molecular Probes) as indicated in figure legends.

Immunofluorescence microscopy. For quantification of DC migration to lymph nodes, lymph nodes were harvested and incubated in 0.05 M phosphate buffer containing 0.1 M L-lysine, pH 7.4, 2 mg mL^{-1} $NaIO_4$, and 10 mg mL^{-1} paraformaldehyde. Twelve hours later, lymph nodes were washed in phosphate buffer and dehydrated in 30% sucrose in phosphate buffer. Tissues were snap frozen in Tissue-Tek (Sakura Finetek). Frozen sections (50 μm) were stained with the indicated antibodies. Confocal images of whole lymph node sections were obtained using the tiling function of a Zeiss 710 or 780 microscope.

Flow cytometry. Cells were stained with the antibodies described above for 1 h at 4 °C, with the exception of CCR7 staining, which was performed at room temperature. Samples were analyzed using an LSR2 flow cytometer (Becton Dickinson). Data were processed using FlowJo software (Treestar).

MMP-9 measurement. Culture supernatants were obtained from BMDCs after stimulation with OVA or IC, as indicated in the figure legends. Total MMP-9 was measured by ELISA (Duo Set, R&D Systems) according to manufacturer's instructions.

Matrix degradation. Glass coverslips were coated with 10 μg mL^{-1} FITC gelatin (Invitrogen) and cross-linked with 0.5% glutaraldehyde[41]. 2×10^5 DCs were plated onto matrix-coated coverslips and incubated at 37 °C to allow degradation, then fixed with 4% paraformaldehyde (MP-Biomedicals) in PBS and stained with TRITC-phalloidin (Sigma) to outline the cell area. Matrix degradation and cell area were quantitated using Imaris software, and the ratio calculated.

***In vitro* migration assay.** The microfluidic-based migration chamber was fabricated using methods established by Haessler *et al.*[42]. Briefly, source, sink and cell channels were patterned using commercial film masks generated by high-resolution laser photoplotting (CAD/Art Services). Melted 3% agarose was poured onto the mask to create the desired channel pattern. These agarose stamps were incubated in 10% FBS with media for 24 h. Device assembly included laying agarose stamps, channel side down, onto a glass coverslip. A PMMA manifold containing inlet and outlet ports was placed on top of the agarose stamp, and the entire device was secured together with a metal clamp. EGFP DCs were mixed with Purecol bovine collagen I (final concentration 1.7 mg mL^{-1}, Advanced Biomatrix) and loaded into the central channel. The chamber was incubated for 15 min at 37 °C, inverting once to ensure uniform cell distribution during collagen gelatination. Following incubation, a rising concentration of CCL19 (maximum concentration 100 ng mL^{-1}) (Peprotech) was applied to the source channel at 5 μL min^{-1}. The sink channel maintained base media under constant flow at 5 μL min^{-1}. Migratory behavior was imaged on an inverted Zeiss 510 microscope under confocal settings with a 20×, 0.9 NA objective.

doi:10.1038/nm.3709

Intravital imaging of dermal DCs by two-photon microscopy. CD11cEYFP mice were anaesthetized and Qdots A655 (Invitrogen Molecular Probes) administered intravenously to delineate dermal vasculature. Alternatively, rat anti-mouse LYVE-1 (clone 223322; MAB2125, R&D Systems) was covalently conjugated to HiLyte Fluor 594 using labeling kits (AnaSpec) and was administered into the footpad an hour before imaging. Footpad dermal DCs were imaged at 915 nm using a Zeiss 510 microscope, as described previously[43,44]. To create a time-lapse sequence, a 70-μm-thick section of the dermis containing lymphatic vessels was scanned at 3 μm *z* steps every 50 s for 1 h 20 min. Imaging alternated between left and right footpads over an 8-h period comparing footpads into which 50 μL^{-1} of OVA or IC or heat-inactivated serum had been injected 16 h previously. Either OVA was placed into the right footpad and IC into the left footpad or control serum was placed in left footpad and lupus serum placed in right footpad, allowing animals to act as their own controls. The investigator performing the imaging was not blinded to this information. The sample size for each experimental group included at least 3 mice; based on previous imaging studies performed in our laboratory this provides data on >50 DCs.

Mouse serum for *in vivo* studies. Serum was obtained from NZB/W F_1 mice with antinuclear antibodies and nephritis (as evidenced by heavy proteinuria) and aged matched WT (C57BL/6) mice. Heat inactivation was performed at 56 °C for 1 h before administration.

Some lupus sera were depleted of IgG using Nab Protein G spin columns (Thermo Scientific) following the manufacturer's standard protocol.

FITC sensitization dermal DC migration assay. FITC sensitization was used to assess dermal DC migration, as described by Robbiani *et al.*[45]. Ovalbumin or immune-complexed ovalbumin was administered subcutaneously to the base of the tail, the flank or the groin on the right and left side respectively of C57BL/6 mice. This allows comparison of the two experimental conditions within the same animal. FITC (8 mg mL^{-1}, Sigma) was dissolved in equal volumes of acetone and dibutyl phthalate (Sigma) and applied in 25-μl aliquots to clipped dorsal skin. Forty-eight hours after FITC painting, inguinal lymph nodes were harvested with nondraining brachial lymph nodes for comparison. Lymph nodes were homogenized, passed through a 70-μm cell strainer, digested in collagenase A (10 mg mL^{-1})/DNAse I (1 mg mL^{-1}) (Roche) and 2% FBS in PBS for 20 min, and the cells were analyzed by flow cytometry. For the serum transfer model, 200 μL^{-1} of heat-inactivated WT or lupus serum was administered intraperitoneally to C57BL/6 mice 12 h before FITC painting. For MMP-9 blocking studies, an anti-MMP-9 antibody (Ab-1, Calbiochem/Merck Millipore, UK IM09L, clone 6.6B) was given at a dose of 4 mg/kg intraperitoneally 12 h before FITC painting and OVA/OVA-IC administration. An isotype control antibody (mouse IgG_1, ab37355, Abcam) was used at the same concentration as the anti-MMP-9 antibody.

Human serum for *in vivo* studies. Serum was obtained from six patients with SLE, three with low BILAG scores (2–9) and three with high BILAG scores (15–21) and three age- and sex-matched healthy controls. Patient characteristics are detailed in **Supplementary Table 1**. Heat inactivation was performed at 56 °C for 1 h before administration. Samples were obtained with informed consent and approval of the Cambridge Local Research Ethical committee (reference 08/H0308/176).

Image analysis. Both *in vitro* and *in vivo* migration movies were processed using Imaris software (version 6.2). The Snapshot tool was used to generate time-lapse movies (with 6–10 fps playback), still images and track histories. To calculate forward protrusion alignment along the dominate CCL19 gradient, independent images from each group were selected, and the angle feature was applied to 20 cells per field to measure the angle between the leading edge and the dominant CCL19 gradient. To further characterize migration behavior, all DC migration data was analyzed using the 'spots' feature in Imaris. Specifically, *x-y* coordinates for each cell tracked were exported to Microsoft Excel and plotted for spatial trajectories. Using the Imaris 'spots' feature, values for *x* displacement and track straightness were calculated for each individual track and plotted in GraphPad PRISM software. Migratory persistence was calculated by dividing displacement values by total path length. Percent distribution of velocities was calculated from the instantaneous velocities of each cell at each time point and binned over selected values. Average speed values were calculated over the entire movie. All chemotactic metrics were calculated in Excel.

Statistical analysis. Statistical analyses were performed using GraphPad PRISM software. A two-tailed Student's *t*-test was applied, unless otherwise indicated. Results are expressed as means and s.e.m. All experiments were subject to at least three replicates per experimental parameter. No statistical method was used to predetermine sample size, and the experiments were not randomized.

38. Schaefer, B.C., Schaefer, M.L., Kappler, J.W., Marrack, P. & Kedl, R.M. Observation of antigen-dependent $CD8^+$ T-cell/dendritic cell interactions *in vivo*. *Cell. Immunol.* **214**, 110–122 (2001).
39. Lindquist, R.L. *et al.* Visualizing dendritic cell networks *in vivo*. *Nat. Immunol.* **5**, 1243–1250 (2004).
40. Lämmermann, T. *et al.* Rapid leukocyte migration by integrin-independent flowing and squeezing. *Nature* **453**, 51–55 (2008).
41. Bowden, E.T., Coopman, P.J. & Mueller, S.C. Invadopodia: unique methods for measurement of extracellular matrix degradation *in vitro*. *Methods Cell Biol.* **63**, 613–627 (2001).
42. Haessler, U., Pisano, M., Wu, M. & Swartz, M.A. Dendritic cell chemotaxis in 3D under defined chemokine gradients reveals differential response to ligands CCL21 and CCL19. *Proc. Natl. Acad. Sci. USA* **108**, 5614–5619 (2011).
43. Tal, O. *et al.* DC mobilization from the skin requires docking to immobilized CCL21 on lymphatic endothelium and intralymphatic crawling. *J. Exp. Med.* **208**, 2141–2153 (2011).
44. Zinselmeyer, B.H., Lynch, J.N., Zhang, X., Aoshi, T. & Miller, M.J. Video-rate two-photon imaging of mouse footpad—a promising model for studying leukocyte recruitment dynamics during inflammation. *Inflamm. Res.* **57**, 93–96 (2008).
45. Robbiani, D.F. *et al.* The leukotriene C(4) transporter MRP1 regulates CCL19 (MIP-3β, ELC)-dependent mobilization of dendritic cells to lymph nodes. *Cell* **103**, 757–768 (2000).